Supplementary Information

Polarization-Enhanced Absorption to EMI Shielding via Joule Heating in Wood-Derived Carbon Foams

Haoyang Feng[a], Jianming Hong[a], Jiaxiang Zhang[a], Pingping He[b,c], Honghai Zhou[a],

Sai Wang[a]*, Hongna Xing[d], Ruosong Li[b,c]*

a. School of Mechatronic Engineering, Shenzhen Polytechnic, Shenzhen, Guangdong 518055, China

b. School of Chemical Engineering, Northwest University, Xi'an, Shaanxi, 710069, China

c. Xi'an Key Lab of Green Hydrogen Energy Production, Storage & Application Integration Technology, 710069, China

d. School of Physics, Northwest University, Xi'an, Shaanxi, 710069, China
E-mail: wangsai@szpt.edu.cn; ruosongli@nwu.edu.cn

Note S1. Preparation of carbonized wood

Put the natural balsa wood with a size of 4 cm × 4 cm × 1 cm into a mixed aqueous solution (2.5 mol/L NaOH and 0.4 mol L^{-1} Na$_2$SO$_3$) at 60 °C for 7 h, and then immerse the wood pieces in deionized water several times to remove excess chemicals. Put the wood block into hydrogen peroxide solution (2.5 mol L^{-1} H$_2$O$_2$) until the wood block is entirely white, and then immerse the obtained wood block in deionized water several times to remove impurities and chemicals. Put the white wood blocks into a freeze dryer and dry for 16 h to obtain delignified wood blocks.

The delignified wood blocks are pre-carbonized at 260 °C for 6 hours in a drying oven; then carbonized in a tube furnace, the temperature is first raised to 300 °C under an Ar atmosphere throughout the process and then heated to 1000 °C for 6 h for carbonization at a heating rate of 5 °C min^{-1}, and finally a carbonized delignified wood block is obtained.

Note S2. CVD method

(1) Open the high-temperature zone and raise to 200 °C. Inject Ar gas (200 ml/min) and open the low-temperature zone.

(2) At 500 °C, fully open the Ar gas to make safety preparations for the later introduction of dangerous gases.

(3) Raise the temperature in the high-temperature zone to 600 °C and introduce H_2 gas (65 ml/min) to reduce the sample.

(4) At 450°C, the iron phthalocyanine powder situated in the lower-temperature region starts to sublimate and migrates to the higher-temperature zone, resulting in the release of blue-purple smoke. This is the appropriate moment to introduce CH_4 gas (35 ml/min) as a carbon source for the growth of CNTs.

(5) Allow continuous growth for about 20 min. When the blue-purple smoke in the low-temperature region has substantially disappeared, it indicates that the growth of CNTs has ended. Turn off the CH_4 gas and keep the Ar unblocked until the temperature drops to room temperature. The products were Co@CNTs/CW foams.

Note S3. Characterization

Raman spectroscopy (LabRAM HR800) with a 532 nm HeNe laser line and X-ray diffraction with a D8 advance X-ray diffractometer were performed to investigate the structural phase. Additionally, the valence state of surface chemical compositions was analyzed through X-ray photoelectron spectroscopy (ESCALAB 250, Thermo). To examine magnetic properties at room temperature, vibrating sample magnetometry (LakeShore-7400) was employed. Thermal stability and decomposition processes were evaluated using thermogravimetry analysis. The morphology was observed using scanning electron microscopy (JSM-7001) and transmission electron microscopy (JEM 2100), while the density was calculated based on the measured mass and volume.

To determine the electrical conductivity, a four-point probe system (ST2258C, Suzhou Jingge Electronics Co., Ltd, China) was used. The water contact angle was measured through a CAST 2.0 contact angle analysis instrument (Solon Information Technology). The temperature

distribution was observed through an infrared camera, specifically the VarioCAM high resolution (InfraTec GmbH, Germany). The total EMI SE (EMI SE_T) was calculated as the combination of absorption SE (SE_A), reflection SE (SE_R), and multi-reflection SE (SE_M). SE_M can be included in SE_A since the EMWs were continuously reflected within the shield until absorbed. Therefore, EMI SE_T was expressed as:

$$SE_T = SE_R + SE_A \tag{S1}$$

Furthermore, to acquire the EMI SE values, Eqs (2) to (6) were applied to the scattering parameters, specifically S_{11} and S_{21}:

$$R = \left|S_{11}\right|^2 = \left|S_{22}\right|^2 \tag{S2}$$

$$T = \left|S_{21}\right|^2 = \left|S_{12}\right|^2 \tag{S3}$$

$$A = 1 - \left|S_{11}\right|^2 - \left|S_{12}\right|^2 \tag{S4}$$

$$SE_R = -10\log\left(1 - R\right) \tag{S5}$$

$$SE_A = -10\log\left(\frac{T}{1-R}\right) \tag{S6}$$

Note S4. Expression of permeability (μ_i)

$$\mu_i = \frac{M_s^2}{akH_cM_s + b\lambda\xi} \tag{S7}$$

where a and b are constants determined by the material, k is a proportionality coefficient, λ and ζ are magnetostriction constant and elastic strain parameters, respectively.
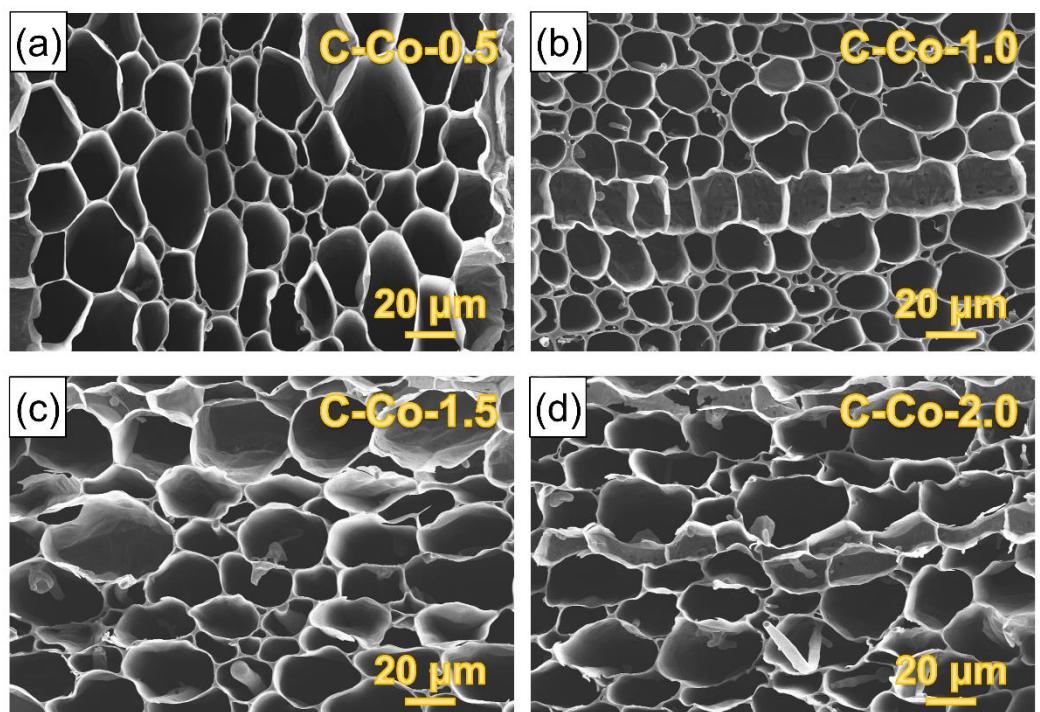
Fig. S1. Cell morphology of (a) C-Co-0.5, (b) C-Co-1.0, (c) C-Co-1.5, and (d) C-Co-2.0.
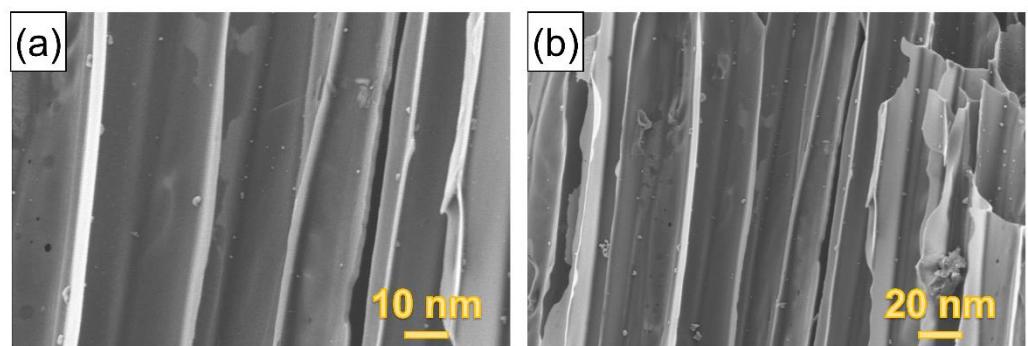

Fig. S2. Structure in the axial (growth direction) directions in Co@CNTs/CW foams.
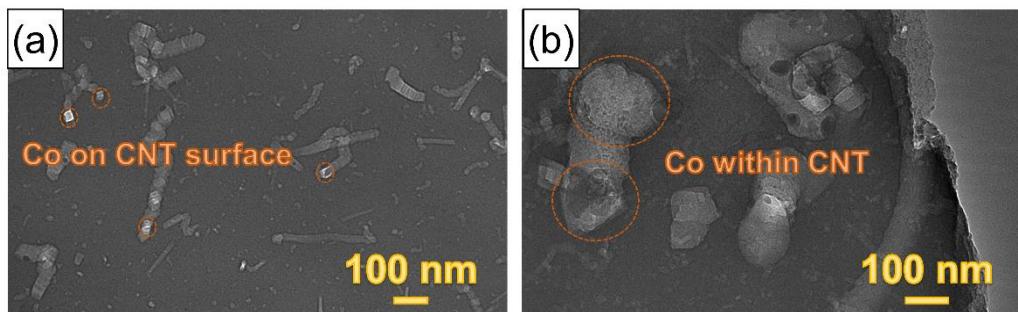
Fig. S3. TEM image of (a) Co nanoparticles on the surface of CNTs and (b) Co nanoparticles encapsulated within CNTs.
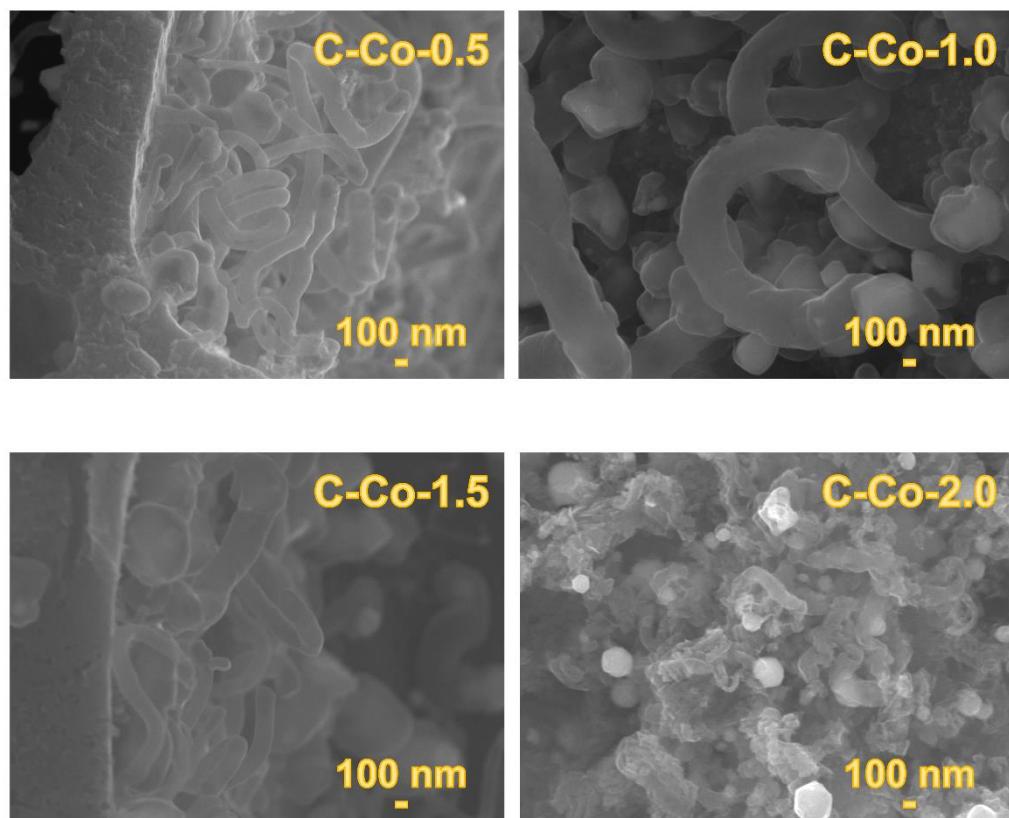


Fig. S4. The size of Co nanoparticles in Co@CNTs/CW foams.
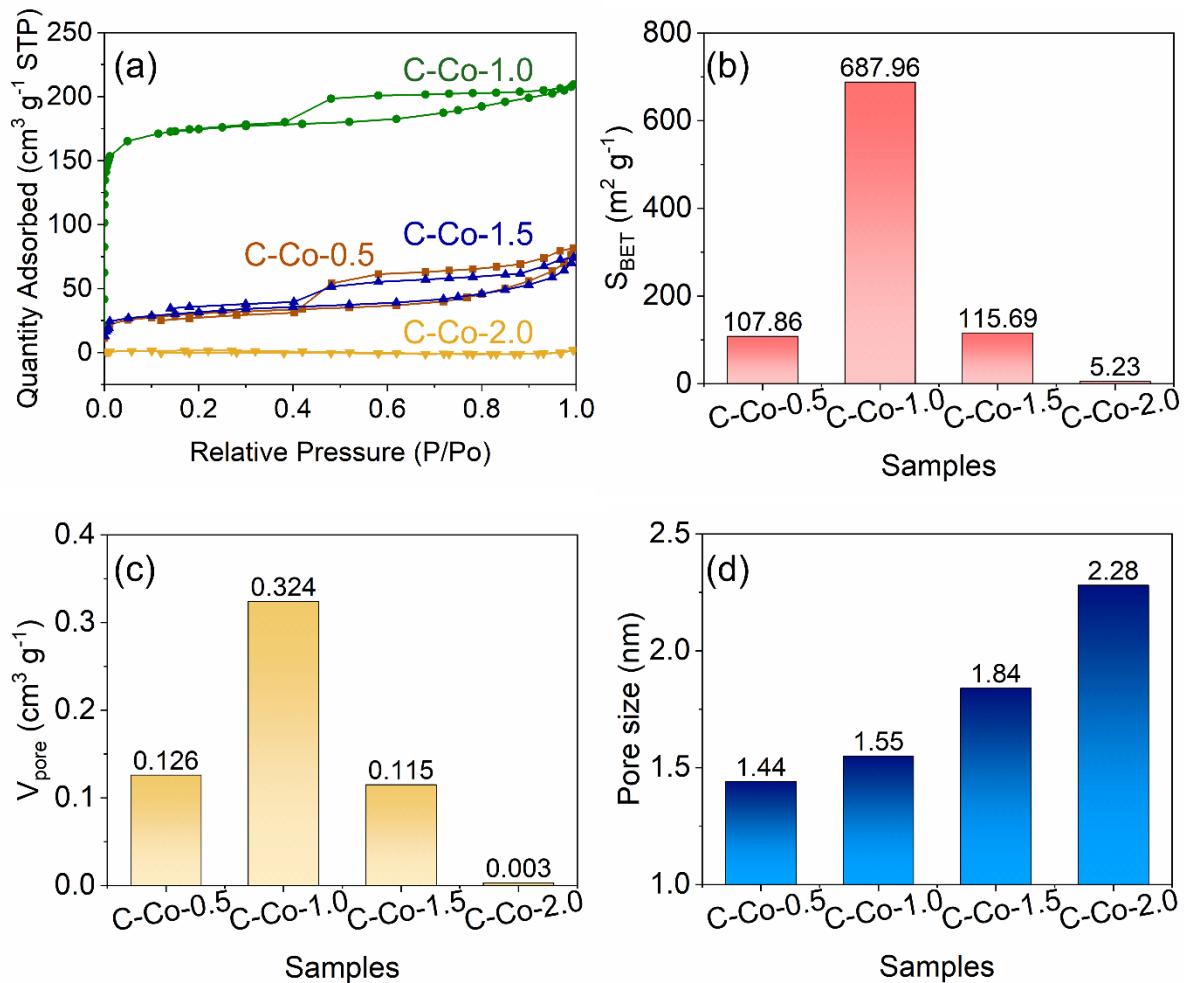
Fig. S5. (a) N_2 adsorption-desorption curve, (b) S_{BET}, (c) V_{pore}, and (d) pore size.
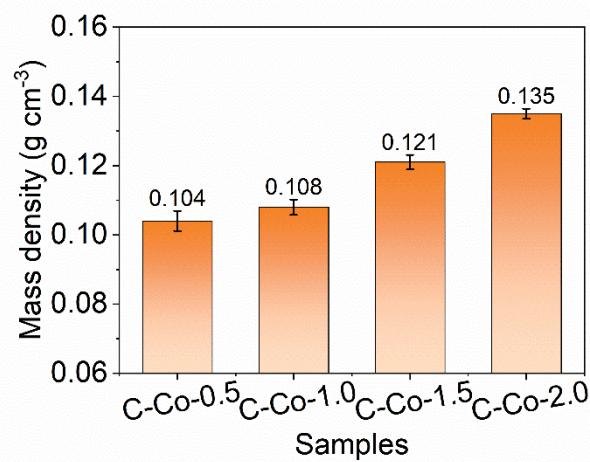

Fig. S6. Mass density of Co@CNTs/CW foams.
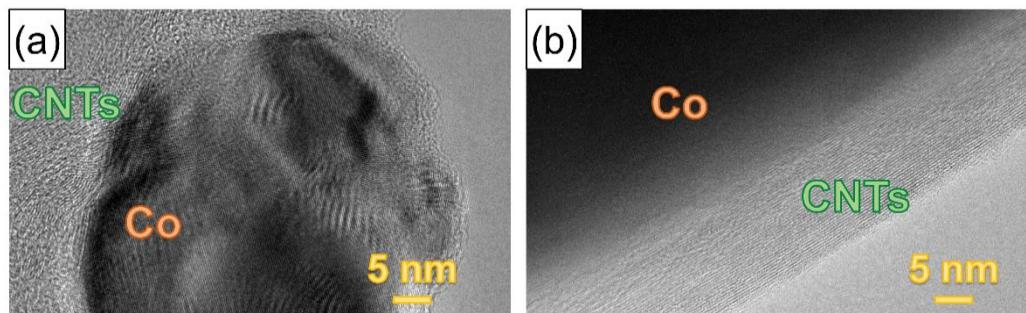
Fig. S7. TEM image of Co sections.
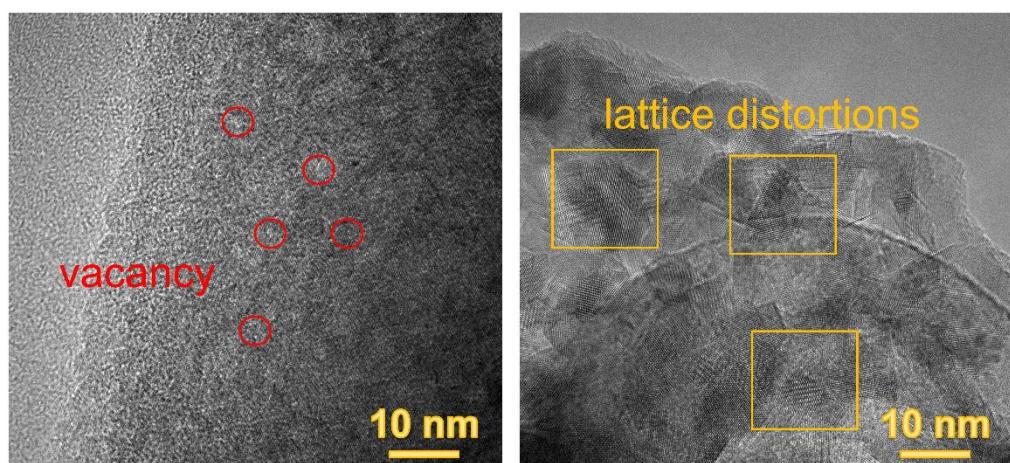

Fig. S8. HRTEM of Co@CNTs.
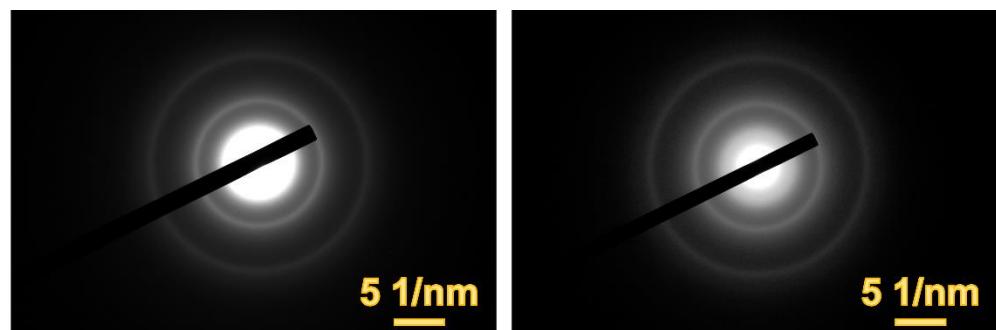
Fig. S9. SAED patterns of CNTs at different regions in Co@CNTs/CW foams.
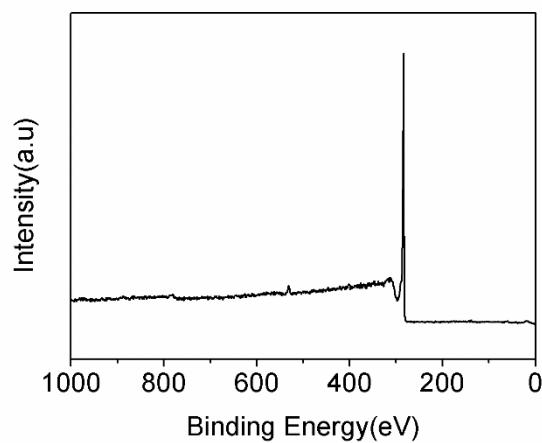
Fig. S10. Full XPS survey.
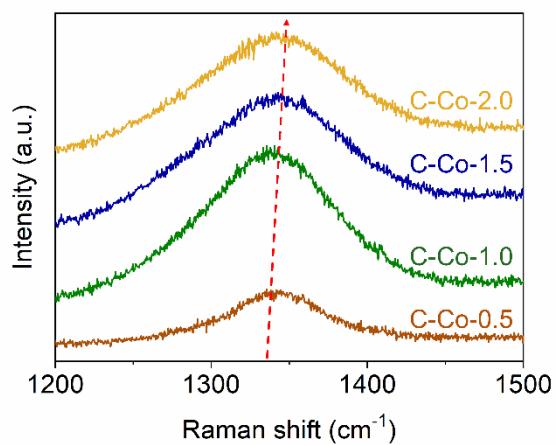
Fig. S11. Center of the D peak of Co@CNTs/CW foams in the Raman shift.
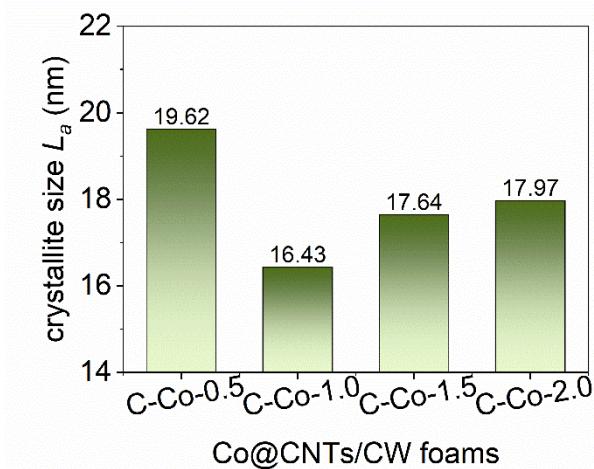
Fig. S12. Graphite crystallite size of Co@CNTs/CW foams.
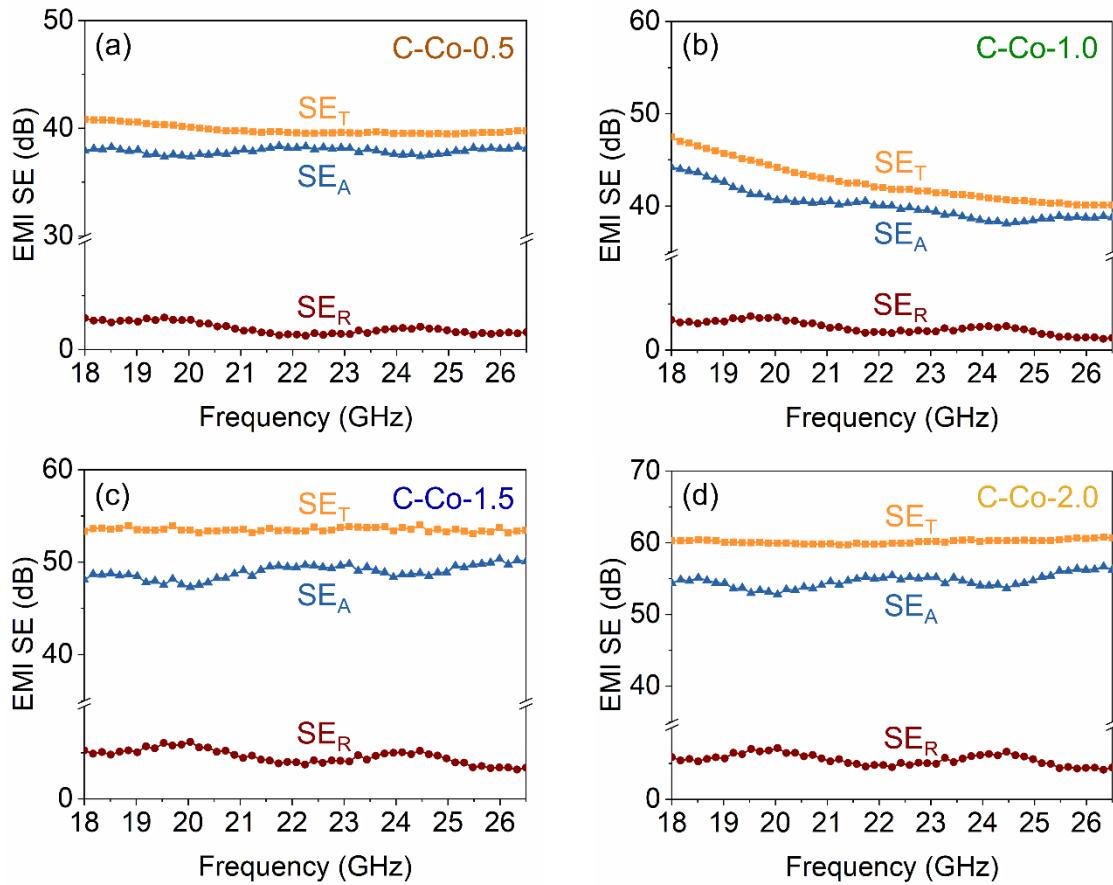
Fig. S13. EMI SE_T, SE_A, and SE_R curves of (a) C-Co-1.0, (b) C-Co-1.0, (c) and C-Co-1.5, and (d) C-Co-2.0.
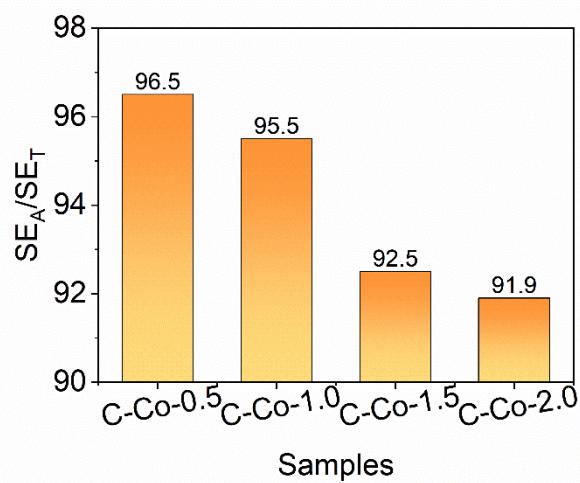

Fig. S14. Ratio of SE_A to SE_T of Co@CNTs/CW foams.
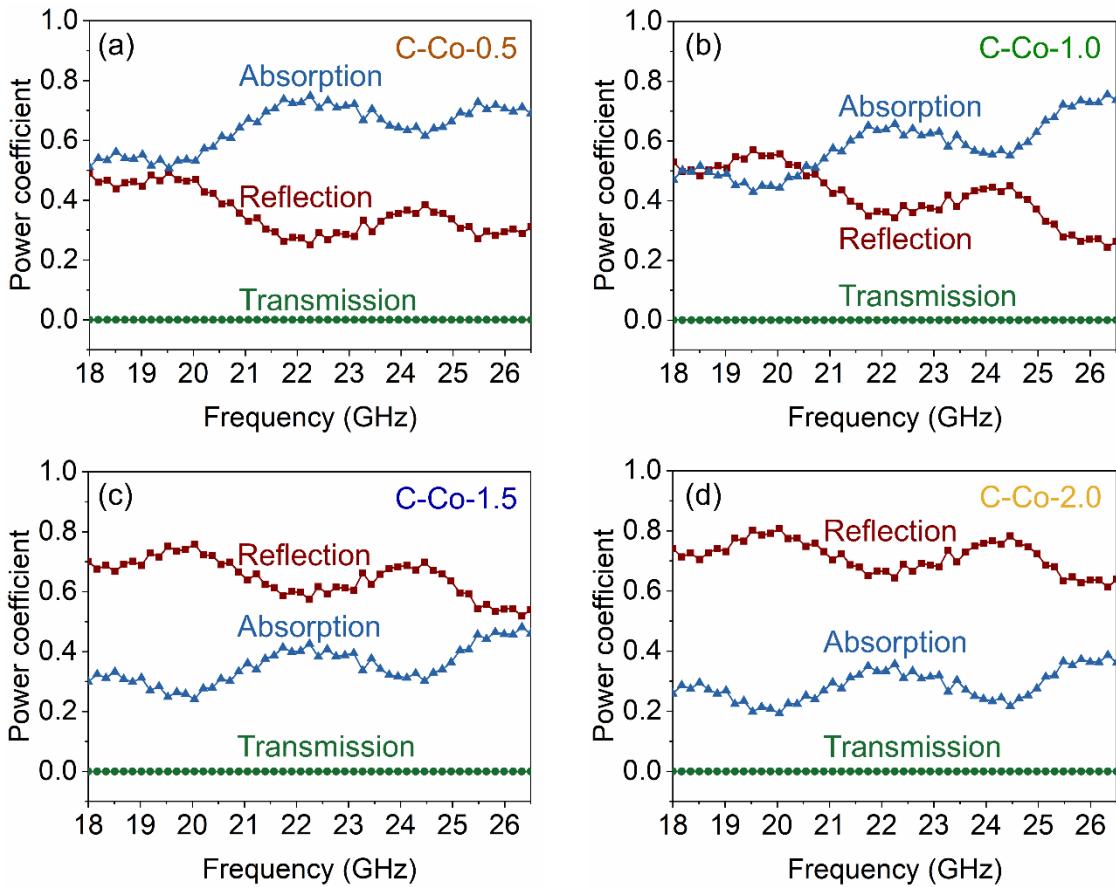
Fig. S15. A, R, and T power coefficient of (a) C-Co-1.0, (b) C-Co-1.0, (c) and C-Co-1.5, and (d) C-Co-2.0.
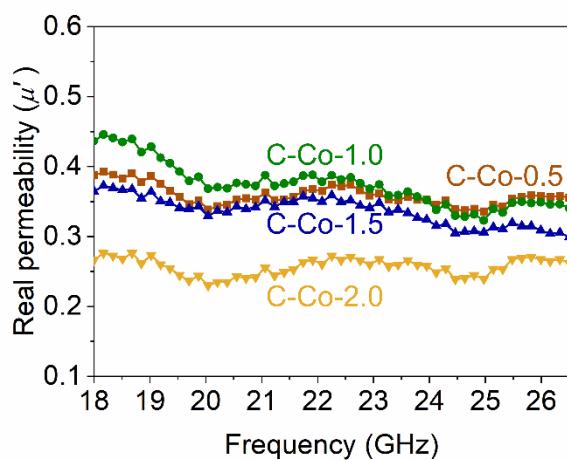
Fig. S16. Real permeability of Co@CNTs/CW foams
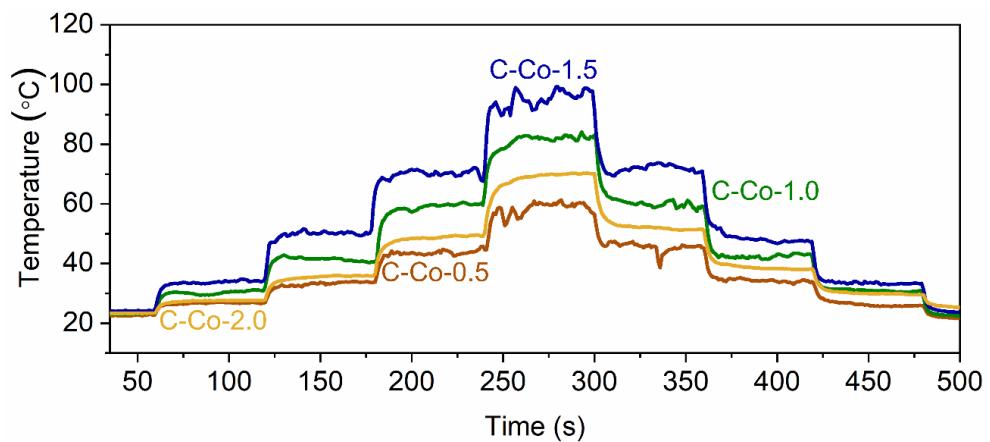
Fig. S17. Temperature profiles under stepwise-increased/decreased input voltages.
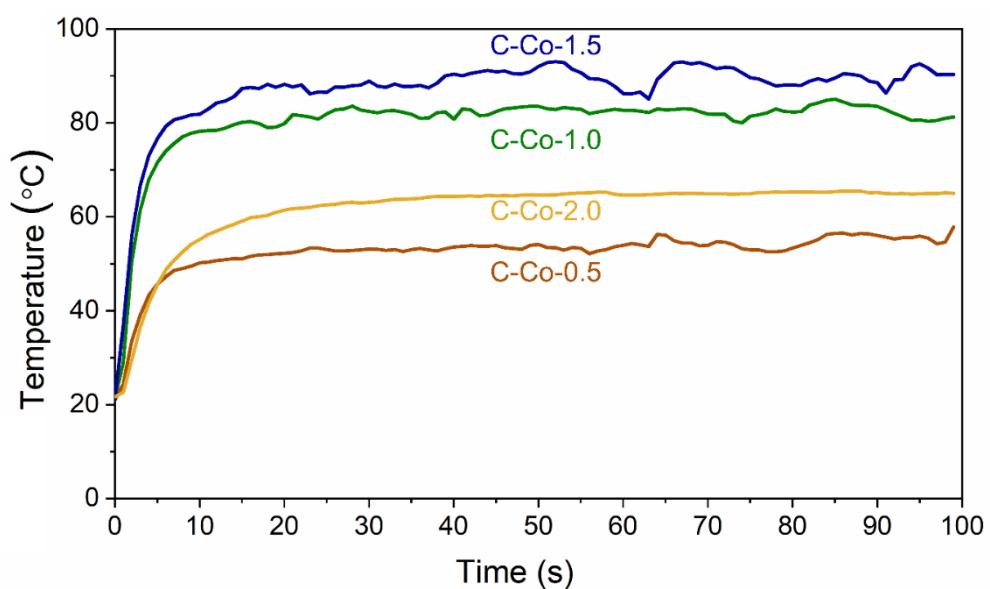
Fig. S18. Long-term time-temperature curve at a constant voltage of 2.5 V.
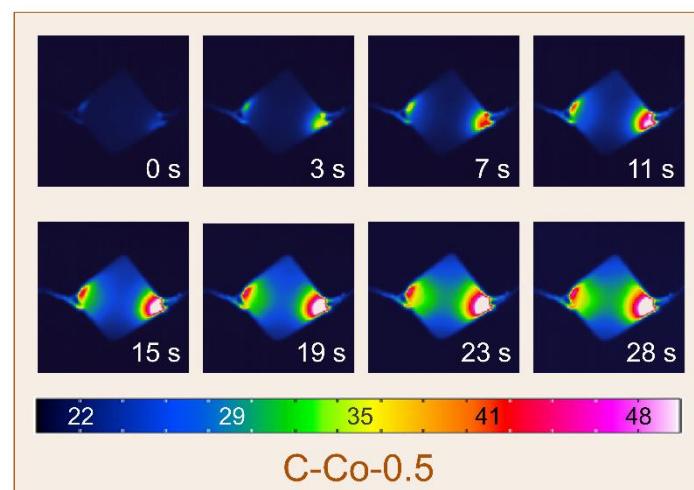
Fig. S19. Infrared thermal images of C-Co-0.5 at an interval of 4 s.
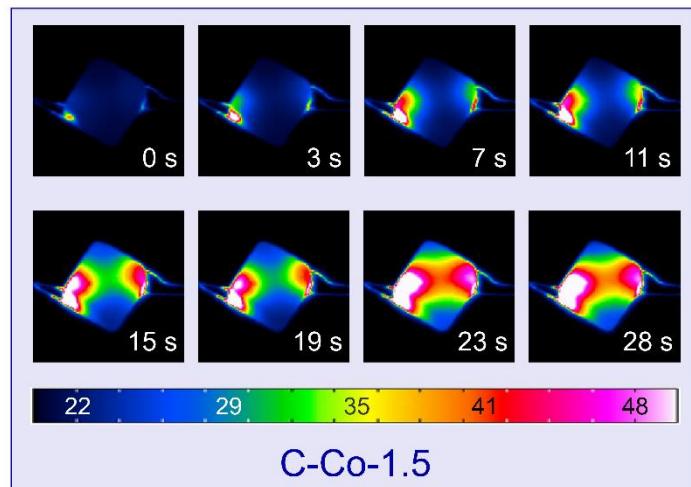
Fig. S20. Infrared thermal images of C-Co-1.5 at an interval of 4 s.
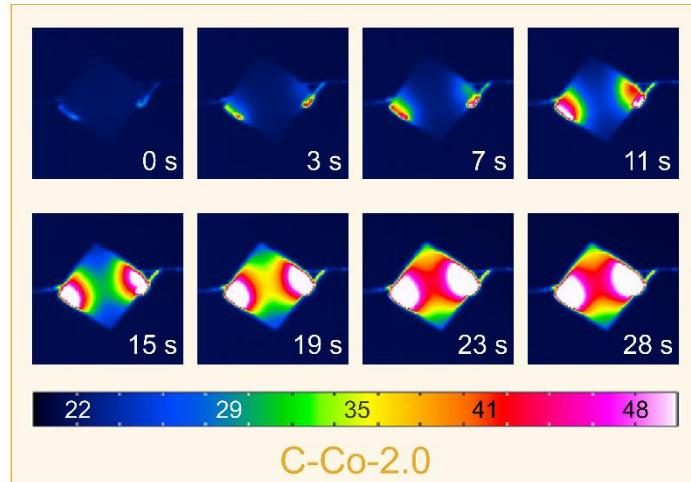
Fig. S21. Infrared thermal images of C-Co-2.0 at an interval of 4 s.
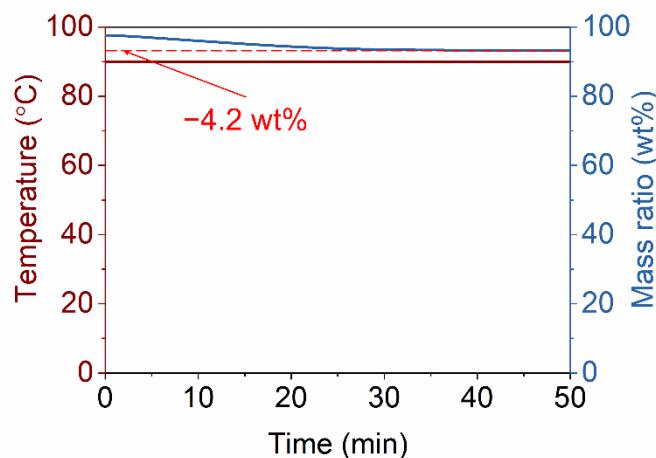
Fig. S22. Mass ratio for Co@CNTs/CW foams (C-Co-1.0) during annealing at 90 °C.
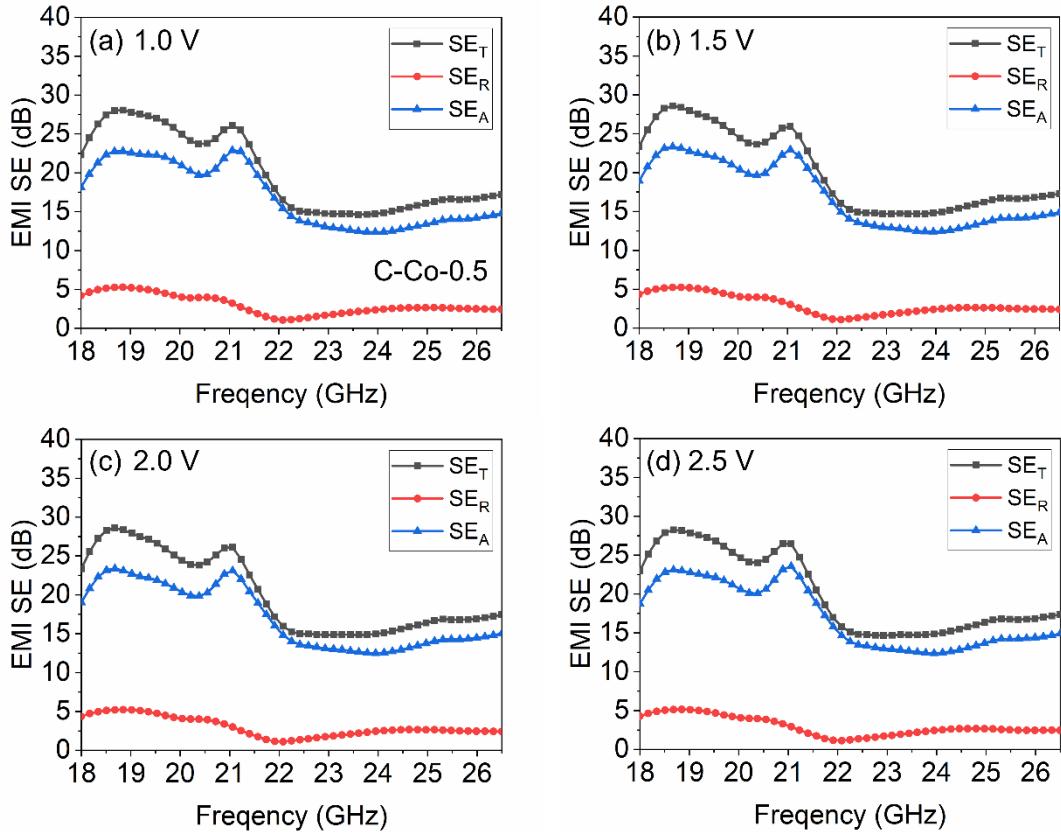
Fig. S23. EMI SE$_T$, SE$_A$, and SE$_R$ curves of C-Co-0.5.
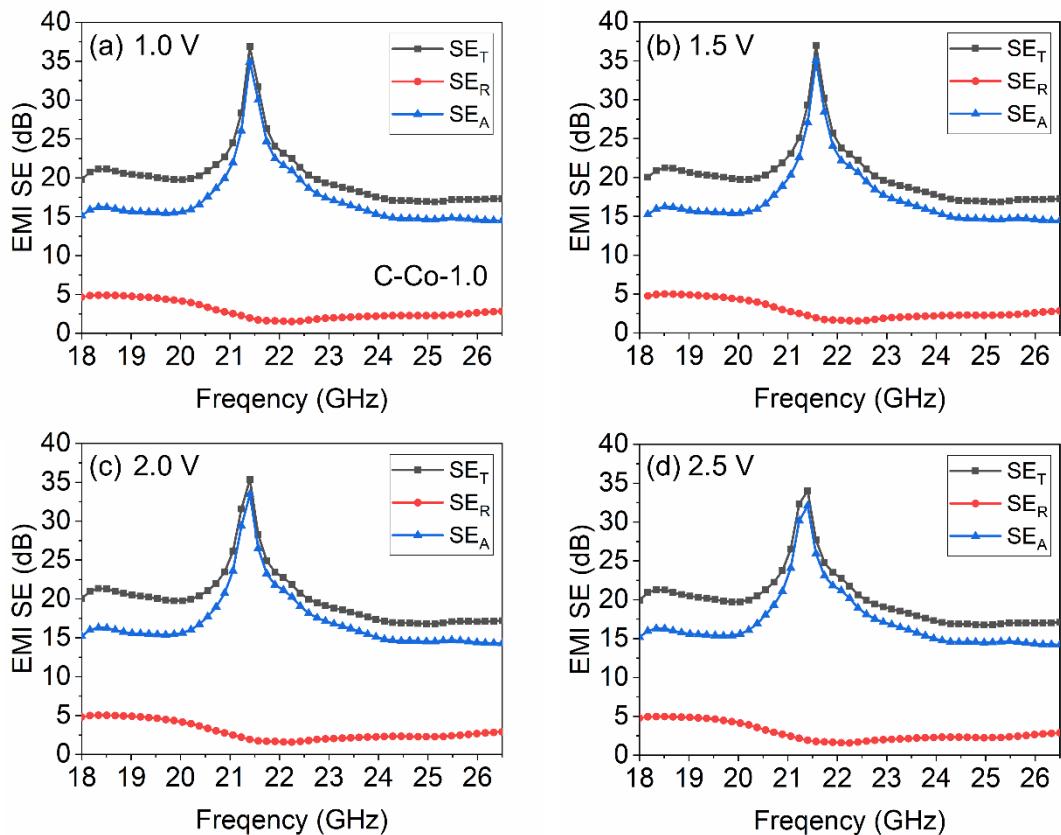
Fig. S24. EMI SE$_T$, SE$_A$, and SE$_R$ curves of C-Co-1.0.
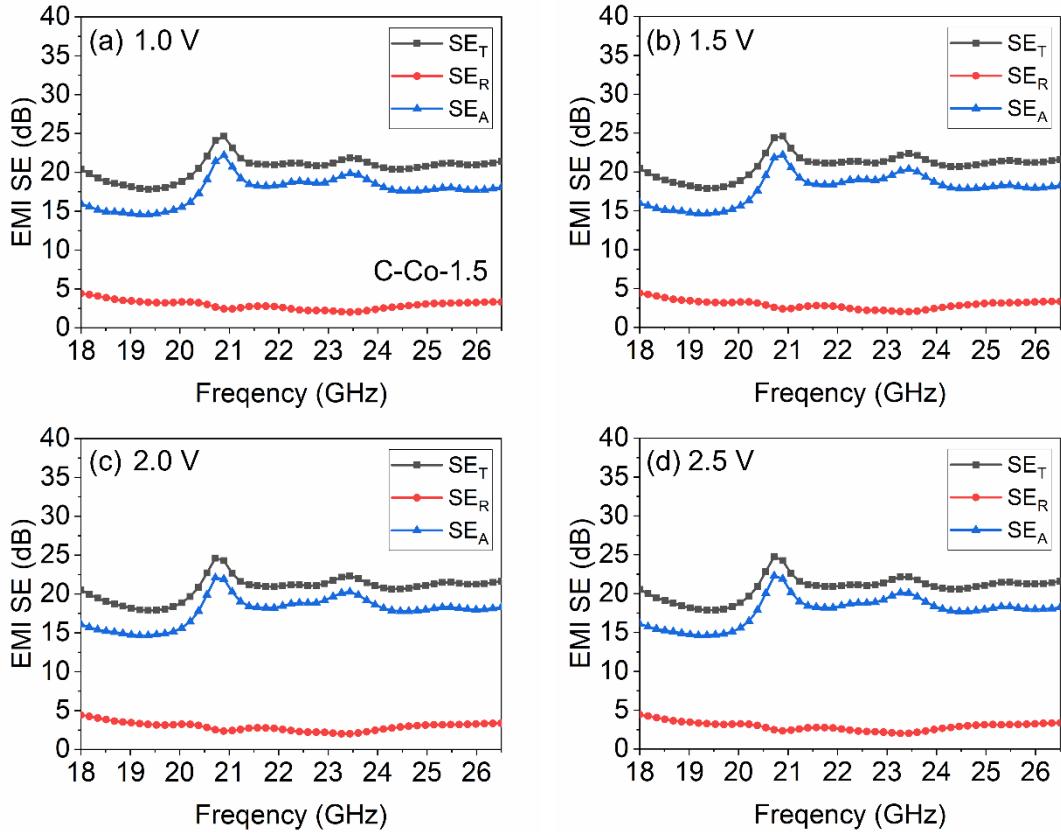
Fig. S25. EMI SE_T, SE_A, and SE_R curves of C-Co-1.5.
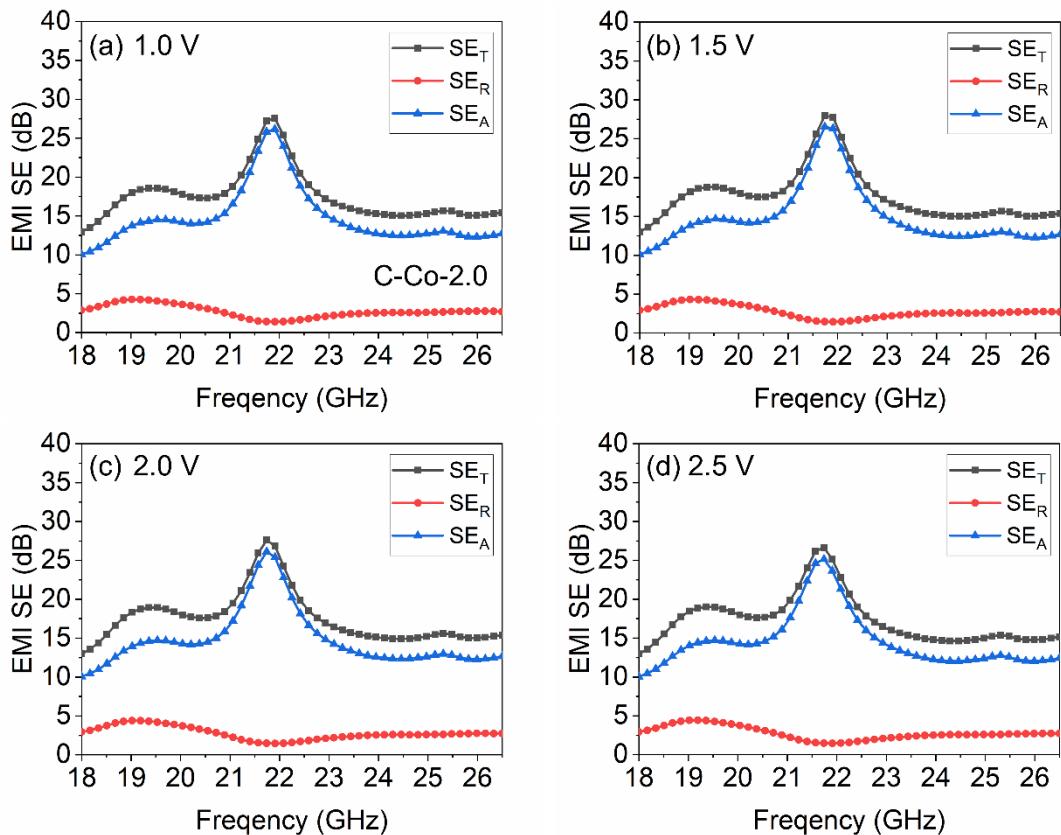
Fig. S26. EMI SE_T, SE_A, and SE_R curves of C-Co-2.0.
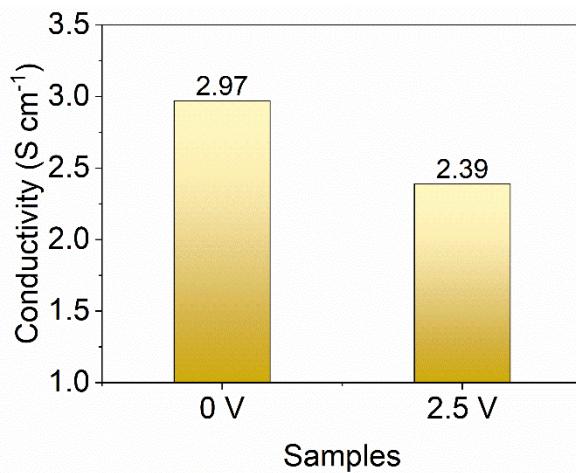
Fig. S27. Conductivity of Co@CNTs/CW foams.
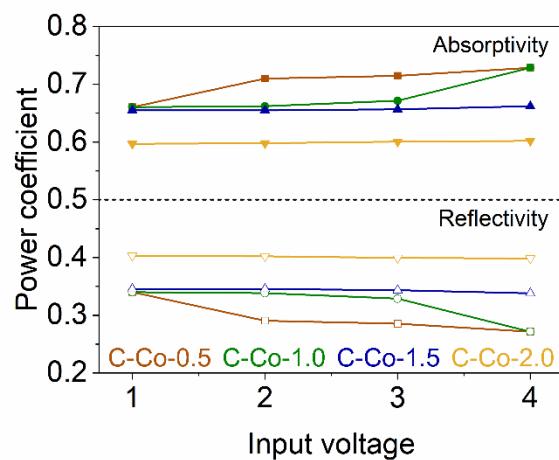
Fig. S28. (a) Reflectivity and (b) absorptivity of Co@CNTs/CW foams.

Table S1. Relationship between Co precursor concentration and Co content

Samples	Co precursor concentration (mol L^{-1})	Co content (wt %)
C-Co-0.5	0.5	7.15
C-Co-1.0	1.0	9.60
C-Co-1.5	1.5	12.8
C-Co-2.0	2.0	18.0

Table S2. Typical EMI shielding performance for some wood-derived and in-situ grown CNT materials

| Type	Shield	SE_T (dB)	SE_R (dB)	Absorptivity	t (mm)	Density (g cm^{-3})	SSE (dB cm^3 g^{-1})	Ref.
Carbonized wood materials	CW/FeCl$_3$@PPy	23	>2.5	0.562	7	0.110	209.09	1
	CW/Ni	50.8	6.5	0.224	2	0.288	176.39	2
	CW/epoxy	27.8	1.1	0.776	2	1.170	23.76	3
	CW/Ni@N-doped CNT	73.7	~5	0.316	2	0.541	136.23	4
	CW/MXene/CNT/PDMS	29.3	6.9	0.204	8	0.150	195.33	5
	CW	63.4	2.2	0.603	3.5	0.290	218.62	6
	CW/TPI/MXene[a]	44.7	~5	0.316	10	0.150	298.00	7
	CW/γ-Fe$_2$O$_3$	44.8	~6	0.251	3	0.271	165.31	8
	CW/Ni	34.1	4.1	0.389	2	0.262	130.15	9
	CW/MXene	61.3	>10	0.100	3	0.197	311.17	10
In situ grown CNT materials	SiC encapsulated Fe@CNT	36.48	~5	0.316	1.8	0.600	60.80	11
	CMF@SiO$_2$-CNT/PDMS[c]	61.34	7.69	0.170	2	/	/	12
	CNT-coated on PAN/Fe$_3$O$_4$	80.0	10.3	0.093	2	1.000	80.00	13
	GF@Ni-CNT[d]	51.0	7.5–10	0.100	0.83	/	/	14
	Pyrocarbon/CNT@graphene	45.3	~12.5	0.056	2.5	1.07	42.34	15
	CW/Ni@CNTs	35.0	~4	0.398	4	0.117	299.15	16
	CF/FeCo@CNTs[e]	41.4	8.3	0.148	4.3	/	/	17
	CW/Co@CNTs	42.0	1.9	0.646	4	0.108	388.89	This study
		59.8	4.8	0.331	4	0.135	442.96	

[a]TPI: trans-l,4-polyisoprene; [b]BF: Basalt fiber fabric; [c]CMF: Carbonated melamine foam; [d]GF: Glass fiber; [e]CF: carbon fiber.

Table S3. Typical EMI shielding, hydrophobicity, and Joule Heating properties in the literature

Shield	EMI SE$_T$ (dB)	SE$_R$ (dB)	Absorptivity	t (mm)	Contact angle (°)	Saturated temperature (°C)	Ref.
PC/MXene/Hf-SiO$_2$ film	20.1	9.4	0.115	2	150.7	100 (13 V)	[18]
MTMS-M/FG[a] composite	57.8	~10	0.100	0.5	138.0	95 (4 V)	[19]
Silicone/MXene/cellulose nanofibers aerogel	39.5	8.4	0.145	0.9	138.0	75 (9 V)	[20]
Polypyrrole/MXene-decorated textile	42.0	/	/	0.43	126.0	79 (4 V)	[21]
Carbonized wood	63.4	2.2	0.603	3.5	13.2	90.2 (2 V)	[6]
Polydopamine/CNTs-coated cotton fabric	23.0	~3	0.501	/	138.0	85 (6 V)	[22]
NR-BP[b]	31.9	~13	0.050	0.05	122.0	155.5 (6 V)	[23]
BC-BP[c]	24.9	~10	0.100	0.036	40.0	124 (6 V)	[24]
MXene/electrospun poly(lactic acid) membrane	55.4	13.6	0.044	0.15	/	52.8 (1.5 V)	[25]
PVDF/MXene/AgNW film[d]	45.4	~10	0.100	/	/	77 (2.5 V)	[26]
CW/Ni	44.3	6.5	0.224	2	152.1	/	[2]
CW/Co@CNT foam	42.0	1.9	0.646	4	140.2	80.5 (2.5 V)	This study
	59.8	4.8	0.331	4	138.6	65.5 (2.5 V)	

[a]MTMS-M/FG: Methyltrimethoxysilane/MXene/wood-pulp fabric grid; [b]NR-BP: natural rubber toughened CNT buckypaper; [c]BC-BP: bacterial cellulose toughened CNT buckypaper; [d]PVDF/MXene/AgNW film: Poly(vinylidene fluoride)/MXene/silver nanowire.

Table S4. Reported work function of Co and CNT in the literature

Materials	Temperature (°C)	Co	Ref.
Co	25	4.89	[27]
	100	4.84	[28]
	205	4.82	[27]
CNT	25	4.50–4.80	[29-31]
	130	4.20	[32]
	200	2.85	

References

1 W. Gan, C. Chen, M. Giroux, G. Zhong, M.M. Goyal, Y. Wang, W. Ping, J. Song, S. Xu, S. He, M. Jiao, C. Wang and L. Hu, *Chem. Mater.*, 2020, **32**, 5280-5289.

2 Y. Zheng, Y. Song, T. Gao, S. Yan, H. Hu, F. Cao, Y. Duan and X. Zhang, *ACS Appl. Mater. Inter.*, 2020, **12**, 40802-40814.

3 Z. Shen and J. Feng, *ACS Sustain. Chem. Eng.*, 2019, **7**, 6259-6266.

4 M. Cheng, W. Ren, H. Li, X. Liu, S. Bandaru, J. Zhang and X. Zhang, *Composites, Part B*, 2021, **224**, 109169.

5 Z. Wang, X. Han, Z. Zhou, W. Meng, X. Han, S. Wang and J. Pu, *Compos. Sci. Technol.*, 2021, **213**, 108931.

6 B. Zhao, P. Bai, S. Wang, H. Ji, B. Fan, R. Zhang and R. Che, *ACS Appl. Mater. Inter.*, 2021, **13**, 29101-29112.

7 X. Jia, B. Shen, L. Zhang and W. Zheng, *Chem. Eng. J.*, 2021, **405**, 126927.

8 Y. Li, S. Yan, Z. Zhang, Y. Liao, H. Rong, R. Zhao and G. Qin, *ACS Appl. Nano Mater.*, 2022, **5**, 8537-8545.

9 T. Gao, Y. Ma, L. Ji, Y. Zheng, S. Yan, Y. Li and X. Zhang, *Adv. Compos. Hybrid Mater.*, 2022, **5**, 2328-2338.

10 C. Liang, H. Qiu, P. Song, X. Shi, J. Kong and J. Gu, *Sci. Bull.*, 2020, **65**, 616-622.

11 H. Mei, X. Zhao, X. Gui, D. Lu, D. Han, S. Xiao and L. Cheng, *Ceram. Int.*, 2019, **45**, 17144-17151.

12 B. Huang, J. Yue, B. Fan, X. Tang, Y. Liu and X. Huang, *Compos. Sci. Technol.*, 2022, **222**, 109372.

13 H. Wei, W. Zheng, Z. Jiang and Y. Huang, *J. Mater. Chem. C*, 2019, **7**, 14375-14383.

14 Y. Liu, D. He, O. Dubrunfaut, A. Zhang, L. Pichon and J. Bai, *Appl. Compos. Mater.*, 2021, **28**, 777-790.

15 L. Feng, Y. Zuo, X. He, X. Hou, Q. Fu, H. Li and Q. Song, *Carbon*, 2020, **168**, 719-731.

16 B. Zhao, P. Bai, M. Yuan, Z. Yan, B. Fan, R. Zhang and R. Che, *Carbon*, 2022, **197**, 570-578.

17 Q. Men, S. Wang, Z. Yan, B. Zhao, L. Guan, G. Chen, X. Guo, R. Zhang and R. Che, *Adv. Compos. Hybrid Mater.*, 2022, **5**, 2429-2439.

18 B. Zhou, Z. Li, Y. Li, X. Liu, J. Ma, Y. Feng, D. Zhang, C. He, C. Liu and C. Shen, *Compos. Sci. Technol.*, 2021, **201**, 108531.

19 X. Jia, B. Shen, L. Zhang and W. Zheng, *Composites, Part B*, 2020, **198**, 108250.

20 W. Xin, M. Ma and F. Chen, *ACS Appl. Nano Mater.*, 2021, **4**, 7234-7243.

21 Q. Wang, H. Zhang, J. Liu, S. Zhao, X. Xie, L. Liu, R. Yang, N. Koratkar and Z. Yu, *Adv. Funct. Mater.*, 2019, **29**, 1806819.

22 J. Ma, Q. Zhao, Y. Zhou, P. He, H. Pu, B. Song, S. Pan, Y. Wang and C. Wang, *Polym. Test.*, 2021, **100**, 107240.

23 M. Fan, S. Li, L. Wu, L. Li, M. Qu, J. Nie, R. Zhang, P. Tang and Y. Bin, *Chem. Eng. J.*, 2022, **433**, 133499.

24 M. Fan, X. Xia, S. Li, R. Zhang, L. Wu, M. Qu, P. Tang and Y. Bin, *Chem. Eng. J.*, 2022, **441**, 136103.

25 Z. Du, K. Chen, Y. Zhang, Y. Wang, P. He, H. Mi, Y. Wang, C. Liu and C. Shen, *Composites Communications*, 2021, **26**, 100770.

26 S. Yang, D. Yan, Y. Li, J. Lei and Z. Li, *Ind. Eng. Chem. Res.*, 2021, **60**, 9824-9832.

27 J. Heras and E.V. Albano, *Thin Solid Films*, 1983, **106**, 275-284.

28 J.M. Heras and E.V. Albano, *Appl. Surf. Sci.*, 1981, **7**, 332-346.

29 S.J. Tans, A.R. Verschueren and C. Dekker, *Nature*, 1998, **393**, 49-52.

30 S.C. Lim, H.J. Jeong, K.S. Kim, I.B. Lee, D.J. Bae and Y.H. Lee, *Carbon*, 2005, **43**, 2801-2807.

31 S. Suzuki, C. Bower, Y. Watanabe and O. Zhou, *Appl. Phys. Lett.*, 2000, **76**, 4007-4009.

32 C.M. Tan, J. Jia and W. Yu, *Appl. Phys. Lett.*, 2005, **86**.